

Electrical transport in nano-thick ZrTe_5 sheets: from three to two dimensions

Jingjing Niu,¹ Jingyue Wang,¹ Zhijie He,² Chenglong Zhang,² Xinqi Li,¹ Tuocheng Cai,¹ Xiumei Ma,¹ Shuang Jia,^{2,3,*} Dapeng Yu,^{1,3} and Xiaosong Wu^{1,3,†}

¹*State Key Laboratory for Artificial Microstructure and Mesoscopic Physics Peking University, Beijing, 100871, China*

²*International Center for Quantum Materials, Peking University, Beijing 100871, China*

³*Collaborative Innovation Center of Quantum Matter, Beijing 100871, China*

Abstract

ZrTe_5 is a new topological material. It exhibits an infamous resistivity anomaly, of which the origin remains elusive. Recently, single layer ZrTe_5 is predicted to be a two-dimensional topological insulator, while experiments have suggested that bulk ZrTe_5 may be a three-dimensional topological Dirac semimetal. We report the first transport study on ultra thin ZrTe_5 flakes down to 10 nm. A significant modulation of the resistivity anomaly by thickness and gating has been observed. Remarkably, the metallic behavior, occurring only below about 150 K in bulk, persists to over 320 K for flakes less than 20 nm thick. We have identified contributions from a semiconducting hole band and a semimetallic band. As the thickness is reduced, the semiconducting band is shifted away from the Fermi level, while the semimetallic band remains. Quantum oscillations reveal that the semimetallic band is a Dirac band with a nontrivial Berry's phase π . By incorporating the Dirac band, the resistivity anomaly of the material can be well explained. Moreover, the effect of the thickness offers a way to tune the energy bands in ZrTe_5 .

The topological insulator (TI) is a new quantum state of matter, which features a topologically protected metallic surface state with an insulating bulk[1, 2]. Although the first experimentally demonstrated topological insulator, HgTe quantum well[3], is a two-dimension (2D) one, the later found three-dimensional (3D) TIs, *e.g.*, Bi₂Se₃ and Bi₂Te₃ families, have been studied the most. This is largely due to easiness in materials growth and the large bulk band gap[4, 5], which are advantageous in both research and technological point of view. However, the unintentional doping of the bulk, generating a sizeable parallel electrical conduction, hinders the understanding and application of the non-trivial surface states[6–8]. On the other hand, 2D TIs will not be affected by the problem owing to their gate tunability[9, 10]. Therefore, there have been great efforts in searching for new 2D TI materials[11–14] and some success has been made in heterostructures[9, 10, 15]. In light of the huge success of 2D crystals, it seems of great interest to find a 2D crystal TI material. Among many theoretical proposals, ZrTe₅ has attracted immediate attention after its prediction[16–21], as it is believed to have a large band gap, ~ 100 meV, and it is a known material.

ZrTe₅ is a layered material in which layers are stacked in the crystallographic b direction. Each layer can be seen as ZrTe₆ prismatic chains in the a direction that are connected by zig-zag Te chains in the c direction. Early studies on ZrTe₅ have found a resistance peak, namely a resistivity anomaly at about 150 K[22]. Although it was originally ascribed to a charge density wave transition[23], later experiments failed to provide evidence for such a transition[24, 25]. The origin of the anomaly remains a mystery. The research has just revived since the prediction of ZrTe₅ being a 2D TI[17–21]. So far, all experimental studies have been focused on bulk ZrTe₅ crystals, while no experiment on ultra thin ZrTe₅ sheets has been reported. As it is monolayer that is predicted to be a 2D TI, it is important to see how the materials evolves with decreasing thickness. Herein, we present experimental investigation on ultra thin ZrTe₅ sheets. A striking modulation of the resistivity anomaly by thickness and carrier density has been observed. Through temperature dependent transport and quantum oscillations, it is shown that a massless Dirac semimetallic band coexists with a semiconducting band at the Fermi level E_F . More intriguingly, with reducing thickness, the semiconducting band shifts away, leading to a single Dirac band at E_F . The presence of the Dirac band provides the crucial element to understand the resistivity anomaly of the material. The results also demonstrate a way to tune the band structure of ZrTe₅.

ZrTe₅ single crystal was grown by an iodine vapour transfer method[22]. The crystallo-

graphic structure was confirmed by X-ray diffraction and transmission electron microscopy (TEM). Raman spectra show the characteristics of ZrTe_5 . Ultra thin sheets were prepared by mechanical exfoliation onto silicon substrates with 285 nm SiO_2 . They can be reliably identified by polarized light owing to their quasi-one-dimensional nature. The thickness of sheets was measured by atomic force microscopy (AFM). Multi-electrode devices were prepared by e-beam lithography processes. Low temperature transport measurements were carried out using a standard lock-in method in a OXFORD variable temperature cryostat.

Fig. 1a shows the high resolution TEM image of a thin sheet exfoliated from a ZrTe_5 crystal. The sharp diffraction spots indicate the high crystalline quality of the sample. Based on the diffraction pattern and the TEM image, we calculate the lattice constants of $a = 0.38 \pm 0.01$ nm, $b = 1.43 \pm 0.01$ nm, $c = 1.37 \pm 0.01$ nm. Raman spectra reproduce characteristic peaks reported for the material[26]. With decreasing thickness, the frequencies of the peaks remain unchanged, whereas the intensity is marked enhanced. Such enhancement of spectrum can be explained by an interference effect due to multi-reflection[27]. However, the enhancement of the peak at 86 cm^{-1} seems much stronger than others. This mode is connected with the vibrational mode of the Te zig-zag chain and it becomes stronger at low temperatures when the material displays metallic behavior[25]. This is very similar to our experiments, where enhancement was observed for thin flakes, which are more metallic, which will be shown later. We also want to point out that the peak at 115 cm^{-1} is almost constant. The implications of these features are not clear and require further study. Instead, we concentrate on electrical transport.

Due to its quasi-one-dimensional nature, exfoliated flakes of ZrTe_5 mostly exhibit rectangular shapes. In addition, the thickness is often non-uniform, manifested as stepped surfaces, shown in Fig. 1d. Consequently, it is difficult to obtain uniform thin sheets in large size. Nevertheless, we sometime observed single layers confirmed by AFM, see supplementary materials. Unfortunately, these single layers lost the optical and Raman characteristics of ZrTe_5 and were electrically non-conducting. In this work, we limit our scope to sheets thicker than 10 nm.

The resistivity of our thick ZrTe_5 flakes as a function of temperature displays a maximum at about 145 K, consistent with the well-known resistivity anomaly in bulk crystals[22]. However, as the thickness t reduces, the temperature of the resistivity peak T_p substantially shifts to higher temperature, shown in Fig. 2a and b. The increase of T_p is significant, as it

reaches 320 K at 20 nm. Below 20 nm, samples turn into metallic in the whole temperature range. For some samples with larger size, we were able to fabricate Hall bars and extract the carrier density from the low field Hall coefficient. In Fig. 2c, we plot the carrier density n as a function of t . To exclude the influence of carrier density variation of bulk samples, we group the samples that were peeled off and patterned in the same batch. We see a clear trend that n increases with decreasing t . If we assume that the total number of electron per unit volume is independent of t , the change of n clearly indicates more than one bands at the Fermi level. As t is reduced, these bands shift in energy, leading to redistribution of electrons among the bands. For flakes thicker than 15 nm, the Hall resistance at higher field starts to deviate from the low field linear dependence, see supplementary materials. This indicates contribution from another band, corroborating with the evolution of n . When the flake is less than 15 nm, the Hall resistance is completely linear, suggesting that only one band remains at the Fermi level, while the other shifts away.

To gain more insight into the properties of ZrTe_5 thin flakes, we apply a gate voltage to tune the carrier density. Both back-gating and ionic liquid top-gating has been performed and similar results were obtained. Since ionic gating offers a much larger carrier density range, we mainly present the data by this method. The temperature dependent resistivity at different gate voltages for three samples with thickness of 14, 28 and 40 nm are plotted in Fig. 3a, b and c. With increasing gate voltage, T_p first decreases and then increases. The non-monotonic dependence has been observed in all samples. Hall measurements were also carried out to obtain the carrier density. A sign reverse in Hall coefficient is observed, indicating a transition of carrier from holes to electrons. The carrier density n is then extracted. In the vicinity of the transition, the Hall coefficient becomes small. n cannot be correctly calculated. Instead, it is interpolated from the n versus the gate voltage V_{Tg} relatively away from the transition point (see supplementary materials). T_p is plotted against n in Fig. 3d, e and f. For all three samples, the minimum T_p occurs close to the charge neutrality point. It is worthy to note that even at the charge neutrality point, the resistivity exhibits metallic temperature dependence at low temperatures, which strongly indicates semimetallicity.

Magnetoresistance measurements further reveal the nature of this semimetallic state. Fig. 4 shows the resistivity of a 15 nm thick sample as a function of the magnetic field up to 14 T. The sample shows a positivity magnetoresistance, which is often seen in Dirac materials.

On top of this magnetoresistance, oscillations are discernible. After subtracting a smooth background, the oscillations are plotted against $1/B$, which display perfect periodicity. They are Shubnikov-de Haas oscillations, which can be described by[28]

$$\frac{\Delta\sigma}{\sigma(B=0)} = \frac{5}{2} \left(\frac{B}{B_f} \right)^{1/2} R_T R_D \cos \left[2\pi \left(\frac{B_f}{B} + \gamma - \delta \right) \right] \quad (1)$$

where σ is the conductivity, $\Delta\sigma$ is the oscillation part of σ , B_f is the magnetic frequency of the oscillations and $\delta = \pm 1/8$ in 3D. R_T describes the temperature damping and R_D describes disorder broadening. $\gamma = 0$ when the Berry's phase is π , while $\gamma = 1/2$ when it is 0. Through the phase of the oscillations, the Berry's phase can be determined. This can be done by assigning the minimum of $\Delta\sigma$ an integer number and plotting the number as a function of $1/B$, the so called Landau plot. Extrapolation of the plot to $1/B = 0$ conveniently gives the Berry's phase, *i.e.*, 0 for Berry's phase of 0 and $1/2$ for a nontrivial phase of π . This technique has been widely employed to identify Dirac electrons in graphene[29, 30], topological insulators[31] and 3D Dirac semimetals[32]. In practical, resistance is usually what is measured. The ambiguity in choosing either maxima or minima of resistivity arises, as the resistivity oscillations $\Delta\rho_{xx}$ can be in or out of phase with $\Delta\sigma_{xx}$, depending on whether $\rho_{xx} > \rho_{xy}$ or $\rho_{xx} < \rho_{xy}$. It can be understood by the conductivity tensor relation, $\sigma_{xx} = \rho_{xx}/(\rho_{xx}^2 + \rho_{xy}^2)$. In a simple single band, $\rho_{xx} < \rho_{xy}$ is always satisfied under the condition for formation of Landau levels $\omega\tau > 1$. Here ω is the cyclotron frequency and τ is the quantum life time, which is always shorter than the transport time. Thus, ρ_{xx} is in phase with σ_{xx} . However, $\rho_{xx} > \rho_{xy}$ can occur even when $\omega\tau > 1$, for instance, in presence of multi-band, parallel conduction or large magnetoresistance. As a result, ρ_{xx} would be out of phase with σ_{xx} , so resistivity maxima should be chosen in the Landau plot[33]. For the sample in Fig. 4, since $\rho_{xx} > \rho_{xy}$, we choose the resistivity maxima. By plotting the Landau index with $1/B$, we find an intercept of 0.66, indicating a Berry's phase of π .

The damping of the oscillation amplitude with temperature is given by the prefactor R_T in Eq. (1). $R_T = \lambda / \sinh(\lambda)$, where $\lambda = 2\pi^2 k_B T m^* / \hbar e B$. Here, k_B is the Boltzmann constant, e is the elementary charge and m^* is the cyclotron mass. As depicted in Fig. 4d, we have fit the temperature dependence of the amplitude to the equation of R_T , yielding $m^* \sim 0.07m_0$, where m_0 is the free electron mass. Assuming a linear dispersion, we have $\hbar k_F = m^* v_F$. The Fermi velocity is estimated as 5×10^5 m/s, in a good agreement with results reported by others[17, 18, 21]. Our analysis of the quantum oscillations strongly supports a massless

Dirac band, which agrees well with recent experiments on bulk ZrTe_5 [17–19, 21].

Combining all the experimental observations, a consistent picture can now be formed. From the thickness dependence of the carrier density, it can be inferred that for thicker flakes, there are more than one bands at the Fermi level, which is consistent with early studies on bulk crystals[34, 35]. Deviation of the Hall resistance from linear dependence at high magnetic field also support presence of at least two bands. The gate dependence of the Hall coefficient reveals a carrier type transition from hole to electron. Moreover, there is no insulating state during the transition. Therefore, it can be conclude that one of the bands is semimetallic. Analysis of the quantum oscillations suggests that the carriers in the band is indeed massless Dirac fermions.

The thickness dependence of the carrier density indicates shifting of bands. With decreasing thickness, one band is pushed out and only the Dirac band remains at the Fermi level according to the Hall resistance. It is interesting how the thickness affects the band structure. First, we note that recent work on other 2D crystals has also discovered that the charge density wave transition can be significantly affected by thickness[36–38]. Recent study on MoS_2 has shown that the interlayer distance increases with decreasing thickness, leading to reduction of interlayer coupling[39]. Second, the first principle calculation has found that the band structure is very sensitive to the lattice constants[16]. In addition, from bulk to monolayer, a direct band gap is transformed to an indirect one. In fact, experiments on bulk ZrTe_5 have found that band shifting with temperature[17, 40]. It is therefore reasonable to understand the band shifting caused by thickness. We propose that the interlayer coupling is reduced in thin flakes, due to expansion in the layer distance. To test it, measurement of the lattice constants with precision is required in future study.

The band picture also explains the resistivity anomaly. For bulk materials, two bands cross the Fermi level. At low temperature, the semimetallic Dirac band dominate the resistivity, giving rise to the metallic behaviour. With increasing temperature, the other semiconducting band takes over, due to either thermal activation or band shifting. The competition of two bands leads to a resistivity peak, of which the temperature depends on the carrier density, as demonstrated by the gating effect. The competition is reflected in the Hall resistance, too. In bulk materials, a sign reversal of Hall and thermopower was found around the resistivity peak[41], *i.e.*, electron-dominated at low T and hole-dominated at high T . However, in thin flakes, the Hall coefficient is positive in the whole temperature

range, shown in Fig. 5, even though the resistivity peak is still present. This is because the Dirac band is now hole-doped due to the aforementioned thickness induced band shifting. By applying a gate voltage, we could tune the Fermi level into the electron side. The sign reversal of Hall with temperature observed in bulk materials is then restored.

In summary, we have studied the thickness and gate dependence of the transport properties of thin ZrTe_5 sheets. A strong modulation of the resistivity anomaly and a semimetallic behaviour have been observed, which provides evidence for presence of two bands at the Fermi level and band shifting resulted from thickness reduction. By analysis of the quantum oscillations, we have identified a massless Dirac band. Our results not only demonstrate tuning the band structure with thickness, but offers a clue to the long-sought explanation of the resistivity anomaly.

We are grateful for enlightening discussion with X. Dai and N. L. Wang. This work was supported by National Key Basic Research Program of China (Nos.2012CB933404 and 2013CBA01603) and NSFC (Project Nos.11074007, 11222436, and 11234001).

* gwljiashuang@pku.edu.cn

† xswu@pku.edu.cn

- [1] Hasan, M. Z. & Kane, C. L. Colloquium: Topological insulators. *Rev. Mod. Phys.* **82**, 3045–3067 (2010).
- [2] Qi, X.-L. & Zhang, S.-C. Topological insulators and superconductors. *Rev. Mod. Phys.* **83**, 1057–1110 (2011).
- [3] König, M. *et al.* Quantum spin Hall insulator state in HgTe quantum wells. *Science* **318**, 766–770 (2007).
- [4] Chen, Y. L. *et al.* Experimental realization of a three-dimensional topological insulator Bi_2Te_3 . *Science* **325**, 178–181 (2009).
- [5] Xia, Y. *et al.* Observation of a large-gap topological-insulator class with a single Dirac cone on the surface. *Nat Phys* **5**, 398–402 (2009).
- [6] Analytis, J. G. *et al.* Two-dimensional surface state in the quantum limit of a topological insulator. *Nat Phys* **6**, 960–964 (2010).
- [7] Checkelsky, J. G., Hor, Y. S., Cava, R. J. & Ong, N. P. Bulk band gap and surface state

- conduction observed in voltage-tuned crystals of the topological insulator Bi_2Se_3 . *Phys. Rev. Lett.* **106**, 196801 (2011).
- [8] Xiu, F. *et al.* Manipulating surface states in topological insulator nanoribbons. *Nat Nano* **6**, 216–221 (2011).
 - [9] Pribiag, V. S. *et al.* Edge-mode superconductivity in a two-dimensional topological insulator. *Nat Nano* **10**, 593–597 (2015).
 - [10] Qu, F. *et al.* Electric and magnetic tuning between the trivial and topological phases in InAs/GaSb double quantum wells. *Phys. Rev. Lett.* **115**, 036803 (2015).
 - [11] Qian, X., Liu, J., Fu, L. & Li, J. Quantum spin Hall effect in two-dimensional transition metal dichalcogenides. *Science* **346**, 1344–1347 (2014).
 - [12] Zhou, J.-J., Feng, W., Liu, C.-C., Guan, S. & Yao, Y. Large-gap quantum Spin Hall insulator in single layer Bismuth monobromide Bi_4Br_4 . *Nano Lett.* **14**, 4767–4771 (2014).
 - [13] Si, C. *et al.* Functionalized germanene as a prototype of large-gap two-dimensional topological insulators. *Phys. Rev. B* **89**, 115429 (2014).
 - [14] Liu, Q., Zhang, X., Abdalla, L. B., Fazzio, A. & Zunger, A. Switching a normal insulator into a topological insulator via electric field with application to phosphorene. *Nano Lett.* **15**, 1222–1228 (2015).
 - [15] Du, L., Knez, I., Sullivan, G. & Du, R.-R. Robust helical edge transport in gated InAs/GaSb bilayers. *Phys. Rev. Lett.* **114**, 096802 (2015).
 - [16] Weng, H., Dai, X. & Fang, Z. Transition-metal pentatelluride ZrTe_5 and HfTe_5 : A paradigm for large-gap quantum spin Hall insulators. *Phys. Rev. X* **4**, 011002 (2014).
 - [17] Li, Q. *et al.* Observation of the chiral magnetic effect in ZrTe_5 . 1412.6543.
 - [18] Chen, R. Y. *et al.* Optical spectroscopy study of the three-dimensional Dirac semimetal ZrTe_5 . *Phys. Rev. B* **92**, 075107 (2015).
 - [19] Chen, R. Y. *et al.* Magnetoinfrared spectroscopy of Landau levels and Zeeman splitting of three-dimensional massless Dirac fermions in ZrTe_5 . *Phys. Rev. Lett.* **115**, 176404 (2015).
 - [20] Zhou, Y. *et al.* Pressure-induced semimetal to superconductor transition in a three-dimensional topological material ZrTe_5 . arXiv:1505.02658.
 - [21] Yuan, X. *et al.* Observation of quasi-two-dimensional Dirac fermions in ZrTe_5 . arXiv:1510.00907.
 - [22] Okada, S., Sambongi, T. & Ido, M. Giant resistivity anomaly in ZrTe_5 . *J. Phys. Soc. Jpn.*

- 49**, 839–840 (1980).
- [23] DiSalvo, F. J., Fleming, R. M. & Waszczak, J. V. Possible phase transition in the quasi-one-dimensional materials ZrTe_5 or HfTe_5 . *Phys. Rev. B* **24**, 2935–2939 (1981).
 - [24] Okada, S. *et al.* Negative evidences for charge/spin density wave in ZrTe_5 . *J. Phys. Soc. Jpn.* **51**, 460–467 (1982).
 - [25] Landa, G., Zwick, A., Carles, R., Renucci, M. & Kjekshus, A. Lacking Raman spectroscopic evidence for a structural phase transition in ZrTe_5 at 141 K. *Solid State Commun.* **49**, 1095–1098 (1984).
 - [26] Taguchi, I., Grisel, A. & Levy, F. Raman scattering in quasi-one-dimensional ZrTe_5 . *Solid State Commun.* **46**, 299–303 (1983).
 - [27] Wang, Y. Y., Ni, Z. H., Shen, Z. X., Wang, H. M. & Wu, Y. H. Interference enhancement of Raman signal of graphene. *Appl. Phys. Lett.* **92**, 043121 (2008).
 - [28] Shoenberg, D. *Magnetic oscillations in metals* (Cambridge University Press, 1984). P. 154.
 - [29] Novoselov, K. S. *et al.* Two-dimensional gas of massless Dirac fermions in graphene. *Nature* **438**, 197–200 (2005).
 - [30] Zhang, Y. B., Tan, Y. W., Stormer, H. L. & Kim, P. Experimental observation of the quantum Hall effect and Berry’s phase in graphene. *Nature* **438**, 201–204 (2005).
 - [31] Qu, D.-X., Hor, Y. S., Xiong, J., Cava, R. J. & Ong, N. P. Quantum oscillations and Hall anomaly of surface states in the topological insulator Bi_2Te_3 . *Science* **329**, 821–824 (2010).
 - [32] He, L. P. *et al.* Quantum transport evidence for the three-dimensional Dirac semimetal phase in Cd_3As_2 . *Phys. Rev. Lett.* **113**, 246402 (2014).
 - [33] Xiong, J. *et al.* High-field Shubnikov de Haas oscillations in the topological insulator $\text{Bi}_2\text{Te}_2\text{Se}$. *Phys. Rev. B* **86**, 045314 (2012).
 - [34] Whangbo, M. H., DiSalvo, F. J. & Fleming, R. M. Electronic structure of ZrTe_5 . *Phys. Rev. B* **26**, 687–689 (1982).
 - [35] Kamm, G., Gillespie, D., Ehrlich, A., Wieting, T. & Levy, F. Fermi surface, effective masses, and Dingle temperatures of ZrTe_5 as derived from the Shubnikov-de Haas effect. *Phys. Rev. B* **31**, 7617–7623 (1985).
 - [36] Goli, P., Khan, J., Wickramaratne, D., Lake, R. K. & Balandin, A. A. Charge density waves in exfoliated films of van der Waals materials: Evolution of Raman spectrum in TiSe_2 . *Nano Lett.* **12**, 5941–5945 (2012).

- [37] Yoshida, M. *et al.* Controlling charge-density-wave states in nano-thick crystals of 1T-TaS₂. *Sci. Rep.* **4**, 7302 (2014).
- [38] Xi, X. *et al.* Strongly enhanced charge-density-wave order in monolayer NbSe₂. *Nat. Nanotechnol.* **10**, 765–769 (2015).
- [39] Cheng, Y., Zhu, Z. & Schwingenschlögl, U. Role of interlayer coupling in ultra thin MoS₂. *RSC Adv.* **2**, 7798 (2012).
- [40] McIlroy, D. N. *et al.* Observation of a semimetal-semiconductor phase transition in the inter-metallic ZrTe₅. *J. Phys.: Condens. Matter* **16**, L359–L365 (2004).
- [41] Littleton, R. T., Tritt, T. M., Kolis, J. W. & Ketchum, D. R. Transition-metal pentatellurides as potential low-temperature thermoelectric refrigeration materials. *Phys. Rev. B* **60**, 13453–13457 (1999).

FIGURES

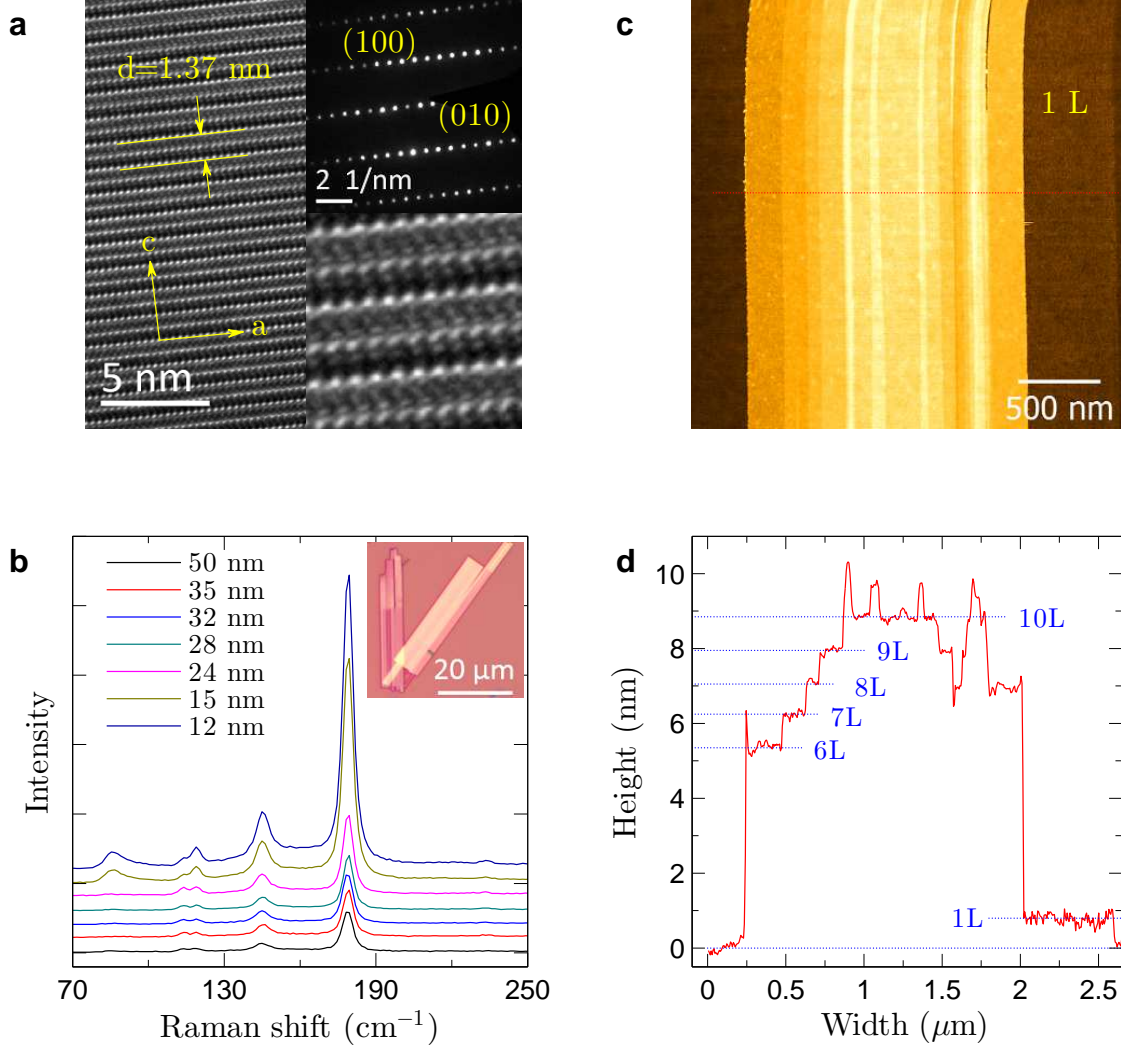


FIG. 1. Exfoliated thin ZrTe₅ flakes. (a) HRTEM image of a thin flake. Bottom-right, a zoom-in image of the left image. Top-right, the electron diffraction looking down the [001] direction. The lattice constants are estimated as $a = 0.38 \pm 0.01$ nm, $b = 1.43 \pm 0.01$ nm, $c = 1.37 \pm 0.01$ nm. (b) Raman spectra at regions of different thickness, measured by AFM. Spectra are shifted for clarity. Inset, the optical image of the measured sample. (c) AFM image of a flake. (d) The line profile shows steps, of which the height corresponds to the layer distance. On the right side, a single layer can be identified by the step height.

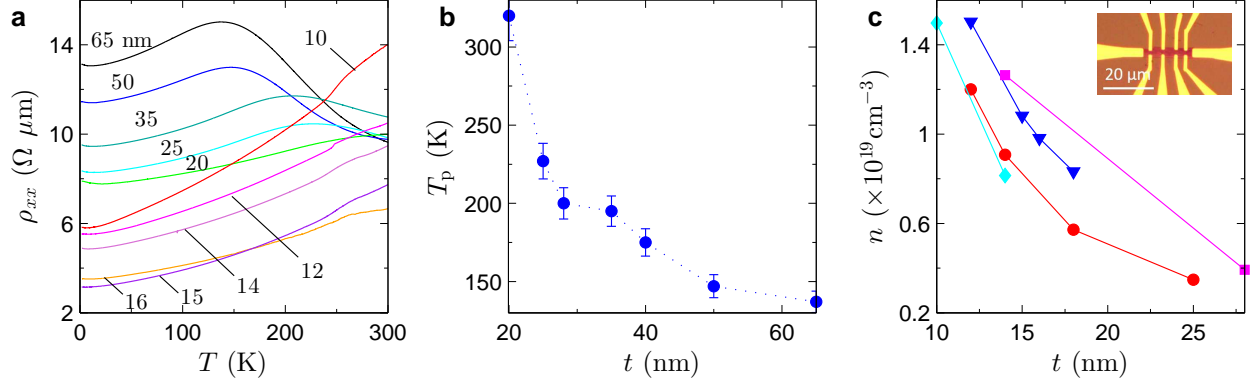


FIG. 2. Thickness dependence of the resistivity anomaly and the carrier density. (a) Resistivity as a function of temperature for flakes of a series of thicknesses. For clarity, not all curves are shown. (b) T_p versus t for flakes thicker than 20 nm. (c) Carrier density as a function of t at 1.5 K. Different colors represent different fabrication batches. Inset, an optical image for a typical Hall bar sample.

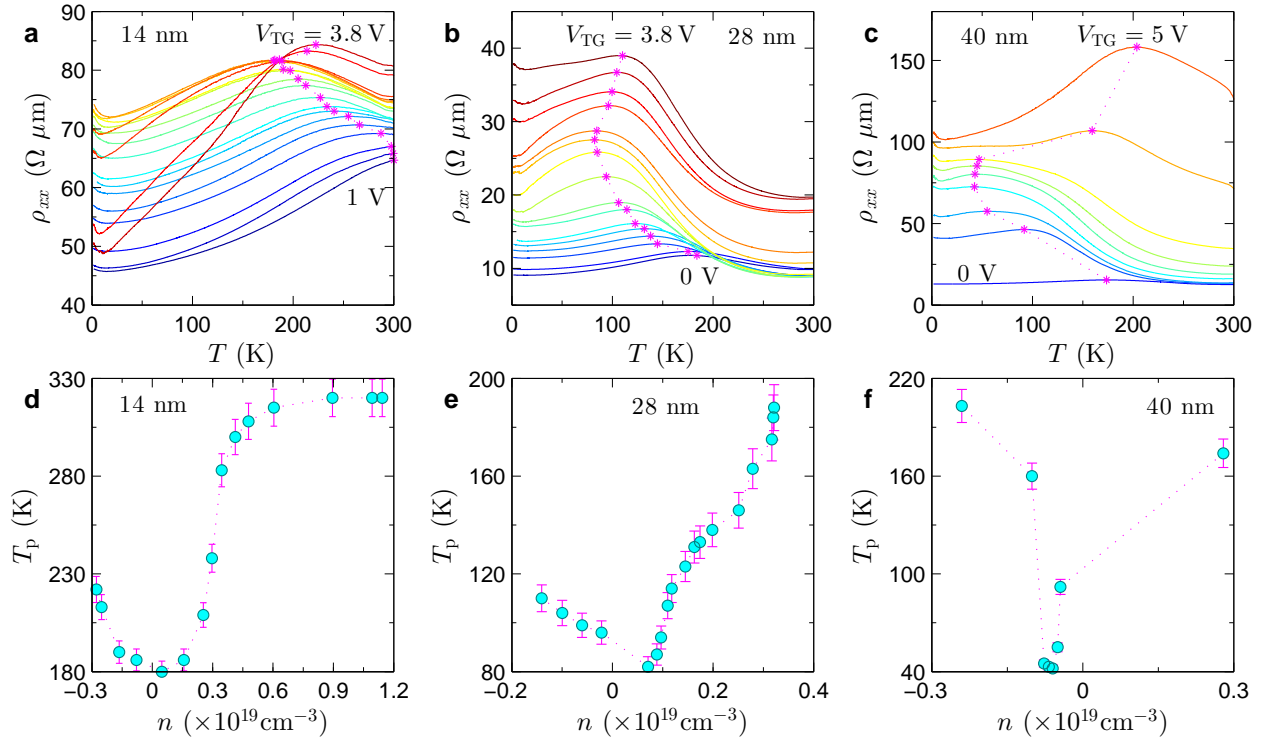


FIG. 3. Gate dependence of the resistivity anomaly. (a)(b)(c) Resistivity as a function of temperature at different gate voltages for three samples with $t=14, 28$ and 40 nm, respectively. In (b), the four curves on the top are shifted up in y axis so as to show the change of T_p . In (c), the top two curves are shifted. The peak temperature T_p is marked by pink *. (d)(e)(f) T_p versus n for the samples in (a)(b)(c), respectively. n is obtained from low field Hall coefficient.

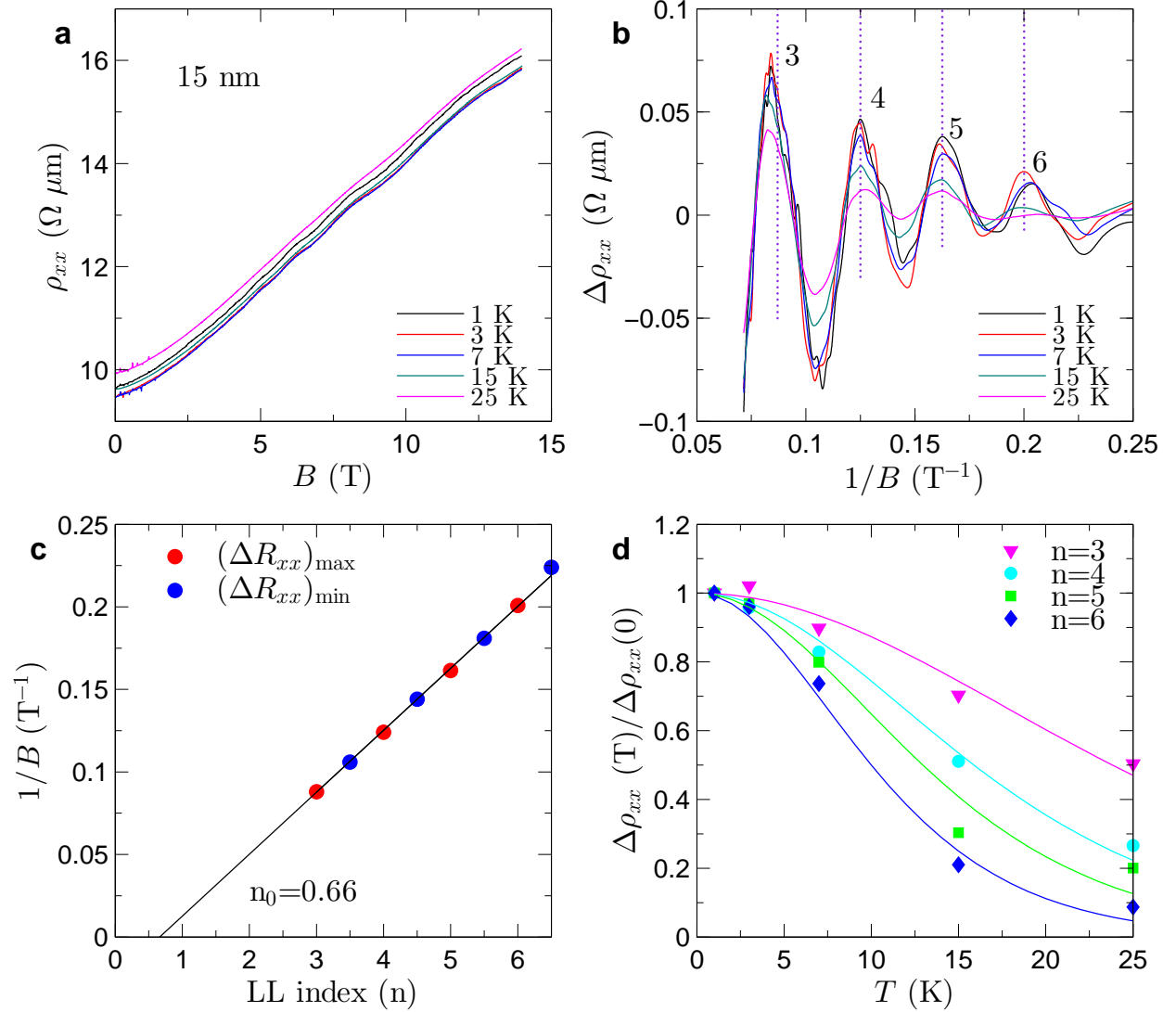


FIG. 4. Quantum oscillations of a 15 nm flake at a backgate voltage of $V_{BG} = 70$ V. (a) Magnetoresistance. (b) Resistivity oscillations as a function of $1/B$ after subtracting a smooth background. (c) Landau plot. The solid line is a linear fit, which extrapolates to x at 0.66, indicating a Berry's phase of π . (d) Damping of the oscillation amplitude with temperature for Landau levels of $n=3, 4, 5$ and 6 . Solid lines are fits to R_T , see the text.

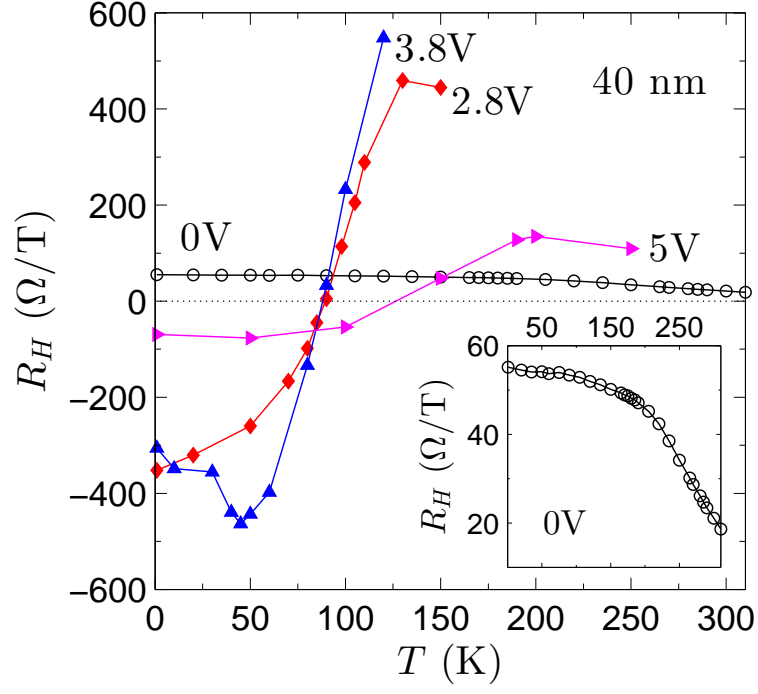


FIG. 5. Temperature dependence of low field R_H at different gate voltages for a 40 nm flake. Inset: re-plot of R_H at $V_{TG} = 0$ V.